A Conserved Coatomer-related Complex Containing Sec13 and Seh1 Dynamically Associates With the Vacuole in *Saccharomyces cerevisiae**⑤

Svetlana Dokudovskaya‡‖‖‖[a], Francois Waharte§, Avner Schlessinger¶, Ursula Pieper¶, Damien P. Devos‖, Ileana M. Cristea**, Rosemary Williams‡‡, Jean Salamero§, Brian T. Chait§§, Andrej Sali¶, Mark C. Field¶¶, Michael P. Rout‡‡‖, and Catherine Dargemont‡‖

The presence of multiple membrane-bound intracellular compartments is a major feature of eukaryotic cells. Many of the proteins required for formation and maintenance of these compartments share an evolutionary history. Here, we identify the SEA (*Se*h1-*a*ssociated) protein complex in yeast that contains the nucleoporin Seh1 and Sec13, the latter subunit of both the nuclear pore complex and the COPII coating complex. The SEA complex also contains Npr2 and Npr3 proteins (upstream regulators of TORC1 kinase) and four previously uncharacterized proteins (Sea1–Sea4). Combined computational and biochemical approaches indicate that the SEA complex proteins possess structural characteristics similar to the membrane coating complexes COPI, COPII, the nuclear pore complex, and, in particular, the related Vps class C vesicle tethering complexes HOPS and CORVET. The SEA complex dynamically associates with the vacuole *in vivo*. Genetic assays indicate a role for the SEA complex in intracellular trafficking, amino acid biogenesis, and response to nitrogen starvation. These data demonstrate that the SEA complex is an additional member of a family of membrane coating and vesicle tethering assemblies, extending the repertoire of proto-coatomer-related complexes. *Molecular & Cellular Proteomics 10: 10.1074/mcp.M110.006478, 1–17, 2011.*

A hallmark of eukaryotic cells is the presence of distinctive internal membrane compartments, dynamically connected via selective transport pathways. Various intracellular transport complexes regulate exchange of material between these compartments and maintain their distinct composition. Recent analyses have suggested that the last common eukaryotic ancestor (LCEA)[1], a hypothetical lineage that gave rise to all modern eukaryotes, and evolved from the first common eukaryotic ancestor by gene duplication and divergence, possessed a highly complex membrane-trafficking system (1, 2). One of the most prominent examples of an evolutionary connection between the internal membrane systems derives from similarities within the architectures of the coat complexes between different classes of coated vesicles (CVs) and between CVs and the nuclear pore complex (NPC) (3–5).

Coated vesicles are membranous transport intermediates encapsulated by distinctive proteinaceous coats. The coat proteins provide structural integrity to vesicle assemblies and mediate communication and exchange of molecules between compartments of the endocytic and secretory pathways. The coat also defines the vesicle type. For example, clathrin, in association with one of four distinct adaptin (AP) complexes,

[1] The abbreviations used are: LCEA, last common eukaryotic ancestor; NPC, nuclear pore complex; COPI, coatomer complex I; COPII, coatomer complex II; HOPS, homotypic fusion and protein sorting; CORVET, class C core vacuole/endosome tethering; TIRFM, total internal reflection fluorescence microscopy; CV, coated vesicle; ER, endoplasmic reticulum; MALDI, matrix-assisted laser desorption ionization; SEA, Seh-1 associated; DTT, dithiotreitol; PIC, protease inhibitor cocktail; GFP, green fluorescent protein.

is involved in endocytosis and trafficking between the Golgi apparatus, vacuole and lysosome, and endosomes. Coatomer complex I (COPI) coated vesicles mediate intra-Golgi movement and are responsible for retrograde transport between the Golgi and endoplasmic reticulum (ER), whereas coatomer complex II (COPII) coated vesicles function in anterograde transport from the ER to Golgi apparatus (6). The common evolutionary origin of these three types of vesicles is supported by the presence of structurally similar elements and mechanisms of vesicle formation, as well as clear common ancestry of multiple subunits within these complexes (5, 7–9).

NPCs are embedded within the nuclear envelope and are the sole mediators of macromolecular nucleocytoplasmic exchange. These structures (~50 MDa in yeast) contain multiple copies of ~30 different nucleoporins or nups. The structural scaffold of the NPC, comprising ~50% of the total NPC mass, is formed almost entirely from proteins consisting of only two folds—α-solenoid-like and β-propellers (4, 10, 11). The same structural modules are present in coated vesicle components. Moreover, the particular arrangement, an amino-terminal β-propeller followed by a carboxy-terminal α-solenoid, has so far only been observed in vesicle coating complexes and NPCs (3) and, with the potential exception of some compartmentalized bacteria, is absent from prokaryotes (12). In both coated vesicles and NPCs these structural folds likely fulfill a similar function, namely to form and stabilize curved membranes. In addition, the β-propeller protein Sec13 is a constituent of both the NPC scaffold Nup84 subcomplex and COPII vesicle coats, in the latter forming a heterodimer with Sec31 (13–15). The similarity between the NPC scaffold nups and vesicle coat proteins extends to the atomic level (reviewed in 16). The presence of shared components, folds and fold arrangements, overall architecture and functions in membrane curvature are the key evidence supporting the hypothesis that CVs and NPCs evolved from a common ancestral protocoatomer (3, 4, 9–11).

If much of the endomembrane system did indeed evolve from an ancestral protocoatomer, it might be expected that additional complexes, structurally related to the coated vesicles and NPC, are present elsewhere within the cell. Indeed, such complexes have been found, and are also predicted to play roles in intracellular transport and/or membrane deformation. One example is the coatomer-related intraflagellar transport complex, required for the assembly and maintenance of cilia and flagella (17). Another complex contains a number of conserved Bardet-Biedl Syndrome proteins (BBSome) and is required for sorting of membrane proteins to primary cilia (18). Two additional complexes containing components with characteristic protocoatomer-like fold arrangements are the multisubunit membrane tethering complexes HOPS (homotypic fusion and protein sorting) and CORVET (class C core vacuole/endosome tethering). These two complexes, collectively termed Vps-C complexes, are associated with vacuoles (lysosomes) and endosomes respectively, and have as yet ill-defined roles in cell control of growth, nutrient transport, autophagy, as well as endosomal and vacuolar assembly and trafficking (19).

Here, we describe a new complex, the SEA (*Seh*1-associated) complex, in the yeast *S. cerevisiae*, which contains Seh1, Sec13, and evolutionarily conserved proteins with predicted secondary structure similarities to components of HOPS and CORVET. The SEA complex is dynamically associated with the vacuole membrane and functional and genetic analyses are consistent with a role for the members of the SEA complex in membrane trafficking and autophagy.

EXPERIMENTAL PROCEDURES

Yeast Strains and Growth Conditions—Yeast strains used in this study are listed in the supplemental Table S1. Yeast were grown to mid-log phase in Wickerham media for immunoprecipitation experiments (0.3% Bacto Malt Extract, 0.3% Yeast Extract, 0.5% Bacto Peptone, and 1% glucose), in yeast nitrogen base media for imaging (0.67% Yeast Nitrogen base without amino acids and carbohydrates, 0.2% complete drop-out mix, and 2% glucose) and in YPD (2% Bacto-Peptone, 1% yeast extract, and 2% glucose) or an appropriate drop-out media for all other purposes. Starvation experiments were conducted in synthetic media lacking nitrogen (SD - N:0.17% yeast nitrogen base without amino acids, 2% glucose).

Immunoprecipitation of the SEA Complex Proteins—SEA complex proteins were genomically tagged with PrA as previously described (20). Affinity purification of SEA complex protein complexes from whole cell lysates using magnetic beads was performed as described previously (10). The extraction buffer used in immunoprecipitation of Seh1-PrA (see Fig. 1) and Sec31-PrA (see Fig. 3*B*, #2) was 20 mM K/HEPES, pH 7.4, 1% Triton, 0.5% sodium deoxycholate, 0.3% sodium *N*-lauroyl-sarcosine, 0.1 mM MgCl$_2$, 1 mM dithiotreitol (DTT), 1:200 dilutions of solution P (2% PMSF, 0.04% pepstatin A in absolute ethanol) and protease inhibitor cocktail (PIC solution) (Sigma, P8340). Beads were washed with 20 mM K/HEPES, pH 7.4, 1 mM EDTA, 0.1% Triton, 0.05% sodium deoxycholate, 0.03% sodium *N*-lauroyl-sarcosine. PrA-tagged Sea1-Sea4, Npr2 and Npr3 (see Fig. 1) were extracted with 20 mM K/HEPES, pH 7.4, 110 mM KOAc, 2 mM MgCl$_2$, 0.1% Tween 20 (TBT buffer), 1% Triton, 75 mM NaCl, 1 mM DTT, as well as 1:200 dilutions of solutions P and PIC. Beads were washed with the TBT buffer, containing 1 mg/ml heparin. Immunoprecipitation of Sea4-PrA in sea3Δ strain (see Fig. 3*B*, #1) was performed with the same extraction and wash buffer (TBT, 1% Triton, 1 M NaCl, 1 mM DTT, 1:200 dilutions of solutions P and PIC). After wash proteins were eluted with 0.5 M NH$_4$OH, 0.5 mM EDTA by incubation for 20 min at room temperature. The eluant was lyophilized, resuspended in SDS-PAGE sample buffer, separated on a 4–20% Tris-glycine gel (Invitrogen), and visualized with Coomassie blue (R-250) staining.

Mass Spectrometry Analysis—Protein bands appearing after Coomassie staining were cut from the gel and prepared for the mass-spectrometry analyses essentially as described in (21, 22). Identification of proteins by mass spectrometry was performed by using matrix-assisted laser desorption ionization (MALDI) MS on either a MALDI Qq-time-of-flight (Sciex) (21) or on a MALDI linear trap quadrupole (LTQ) Orbitrap XL (Thermo) (22). MALDI LTQ Orbitrap MS analyses were acquired for a mass range of *m/z* 700–4000 with the following parameters: resolution setting, 60,000 at *m/z* 400; automated spectrum filter off; 50 scans/step; automated gain control on; allowing storage of 5e^5 ions. The list of singly charged monoisotopic masses was generated using Xtract within Qual Browser (XCalibur,

version 2.0.7) with the following parameters: MH$^+$, *m/z* 700–4000 mass range; resolution, 60,000 at *m/z* 400; and signal-to-noise threshold of peak picking, 2. The lists of putative proteins were obtained by database searching against the National Center for Biotechnology Information nonredundant protein database, version October 16, 2006, using the computer algorithm XProteo, version 1.2 (http://www.xproteo.com). Search parameters for MS data were: species, *Saccharomyces cerevisiae* (11105 sequences); protein mass, 0–300 kDa; protein pI, 1–14; mixture search, auto; number of candidates displayed, 20; enzyme, trypsin; miscleavages, 1; mass type, monoisotopic; charge state, MH$^+$; mass errors, 0.06 Da for analyses performed on the MALDI Q-ToF and 5ppm for those performed on the MALDI LTQ Orbitrap; fixed modification, carbamidomethylation of Cys; and variable modification, oxidation of Met. Gi numbers of identified proteins, protein description, kDa, number of matched *versus* observed masses, protein sequence coverage (%), XProteo scores (d') following database search are listed in supplemental Table S2. An XProteo d' score of 4 reflects a positive rate of 0.99 and false positive rate of 0.05. Only the proteins that were identified with d' > 4 are reported.

PAL and Bioinformatics Analysis—PAL analysis of PrA-tagged Sea proteins was performed as described previously (23). Secondary structure of a query sequence was predicted by PSIPRED (24) from the multiple sequence alignment constructed by two iterations of PSI-BLAST. For fold assignment, the protein sequences were divided into domains based on the PAL data, predicted secondary structure, and the output from the disorder predictions by IUPred (25) and DISOPRED2 (26) (supplemental Table S3). The folds of the full-length sequences and their domains were attempted to be assigned by the threading servers FUGUE (27), pGenTHREADER/mGenTHREADER (28), Phyre (29), and SAM-T08 (30) (using the default parameters) as well as the comparative modeling server ModWeb (http://salilab.org/modweb) (template selection was performed using sequence-sequence, sequence-profile, and profile-profile methods, with an E-value threshold of 1.0) (31). A fold was assigned when at least two of the five servers predicted the same fold with high confidence (*i.e.* FUGUE, ZSCORE ≥ 95%; Phyre, Estimated Precision ≥ 50%; pGenTHREADER/mGenTHREADER, *p* value < 0.01; SAM-T08, E-value < 0.01; MODWEB, Z-DOPE < 0 or sequence identity > 30%). Otherwise, the sequence was also submitted to the I-TASSER server (32); a fold was assigned when high confidence predictions (*i.e.* Norm. Z-score > 1) were similar to those of at least one other server. Some fold assignments were also validated by the corresponding entries in the Pfam database (supplemental Table S3) (33). The most accurate comparative models from ModWeb were selected using several quality criteria, including Z-DOPE (34), MPQS (31), sequence identity, and GA341 (31). The complete model set is available in our MODBASE database (http://salilab.org/modbase/search?dataset = seac) (31). SCOP domain names were used to term assigned folds (http://scop.berkley.edu). PEST sequence analysis (supplemental Table S3) was done by the Epestfind program (http://mobyle.pasteur.fr/cgi-bin/portal.py?form = epestfind).

Comparative Genomics and Phylogenetic Analysis—Representative completely sequenced genomes from five of the Eukaryotic supergroups were searched using *S. cerevisiae* sequences as queries (supplemental Table S5). In some instances validated orthologs were also used to extend search reliability. Details of the genomes selected and relevant addresses for web resources were as previously described (35). Searches were performed either at National Center for Biotechnology Information or locally using either BLAST (http://blast.ncbi.nlm.nih.gov.gate1.inist.fr/Blast.cgi) or Smith Waterman algorithms (36), typically with the BLOSUM45 matrix (37). Orthology required the fulfillment of reverse BLAST, *i.e.* the original query was retrieved as the top, or near top, hit using the candidate sequence as

the new query. In addition, identified ortholog candidates were assessed for domains, domain structure and predicted polypeptide length. Comparative genomics spreadsheet data were converted to a Coulson Plot using CPG v0.5b (http://homepage.mac.com/mfield/lab/cpg/The_Coulson_Plot_Generator.html).

Phylogenetic analysis of the Sea2-Sea4 cluster (supplemental Fig. S1) was done using *M*$_r$ Bayes (38), PhyML (39) and RAxML (40) as described (35). The phylogenetic reconstruction was performed using one or more representative sequences from each supergroup to determine the presence of the proteins across the range of eukaryotes.

Microscopy—Yeast cells carrying proteins of the SEA complex genomically tagged with green fluorescent protein (GFP) or mCherry were grown to mid-log phase in yeast nitrogen base instead of YPD to minimize the auto-fluorescence of the culture media. Cells were placed on Ibidi-dish (Biovalley, Alsace, France, #81156), covered with 1 mg/ml concanavalin A (Sigma #C7275) to prevent cell movement and visualized at room temperature using a spinning disk microscope or total-internal reflection fluorescence microscope.

Steady-state images were obtained on a custom confocal spinning-disk microscope, comprised of a Nikon TE2000-E microscope with a 60× NA 1.4 oil objective, a Coolsnap HQ2 CCD camera (Photometrics, Tucson, AZ), a CSU22 spinning-disk head (Yokogawa), and 491 nm solid-state laser (Errol laser bench). All components were driven by Metamorph software (MDS, Foster City, CA). The small pixel size of the CCD camera allowed the use of a 60× magnification objective instead of a 100× objective, which greatly improved the brightness of images while maintaining a high spatial resolution. Final images were obtained by Sum Intensity Projection of a sequence of 20 images taken at 500 ms exposure time with full laser power.

The dynamics of fluorescent structures was studied using a TIRFM based on a TE2000-E Nikon microscope with 100x CFI Plan Apo VC NA 1.49 oil objective and equipped with 491 nm and 561 nm lasers (Errol laser bench), all components were driven by Metamorph software. Images were collected on a QuantEM EM-CCD camera (Photometrics/Roper) with a Dualview image splitter (Optical Insights) mounted with a GFP/mCherry filter set (Chroma Technology) that allowed simultaneous two-color acquisitions at 50 ms per frame (70 ms for Seh1-GFP). Adjustments of the laser angle at the output of the objective were made to optimize the signal-to-noise ratio.

Image Analysis—DIC image contrast was adjusted using histogram stretching with ImageJ software ("enhance contrast" function with 0% saturated pixel). Contrast of GFP images was manually adjusted to reduce constant background in the image (global increase of lowest intensity value). Time-lapse TIRFM images were treated by a moving/immobile component separation algorithm (41) to extract the motion of subcellular structures from the fluorescent "background" (immobile structures and autofluorescence) and/or by a denoising algorithm (42) to improve signal-to-noise ratio before visualization and interpretation. Correction for photobleaching was done for Seh1 data by the Bleach correction ImageJ plug-in (http://rsb.info.nih.gov/ij/) with decay rate adjusted depending on the acquisition. Kymogram representation was obtained by extracting pixel intensities along a line and making a XT image composed of intensity along the line for each time point. These reconstructed images thus show horizontally the fluorescence intensity along the line and vertically the temporal variation of the intensity for each pixel of the line.

Vacuole Isolation and Carbonate Extractions—Isolation of vacuoles from PrA-tagged strains of SEA complex proteins was done essentially as described in http://faculty.washington.edu/merza/pdf/kj_fusion_6.pdf. For carbonate extraction experiments, vacuole fractions were adjusted to a final concentration of 0.1 M Na$_2$CO$_3$, incubated in ice for 30 min and centrifuged in TLA 100.2 rotor at 100,000$_{av}$ for 30

min. The pellets were resuspended in the loading buffer, whereas supernatants were precipitated with TCA (see the following), resuspended in the same amount of the loading buffer. Proteins from both samples were separated by SDS-PAGE and analyzed by Western blotting.

Subcellular Fractionation and Sedimentation Analysis—Yeast strains of PrA-tagged SEA complex proteins were grown in 1 liter of YPD to $A_{600} = 0.6$–0.8, cells were collected by centrifugation (2000 × g, 5 min), and washed with 100 mM Tris pH 9.4, 10 mM DTT for 10 min at 30 °C. After centrifugation cells were resuspended in 45 ml of YPD, containing 50 mM KPi pH 7.5, 600 mM Sorbitol, and a mixture of lysing enzymes: 20 mg of Zymolyase 20-T (Seikagaku, 120491), 6 mg of Lysing enzyme from *Trichoderma harzianum* (Sigma, L1412), 600 mcl of glusulase (Perkin Elmer NEE 154001EA), and incubated at 30 °C for 30 min. Spheroplasts were collected by centrifugation at 1000 × g for 3 min and washed two times with YPD, 50 mM KPi pH 7.5, 600 mM Sorbitol to remove the rest of lysing enzymes. Spheroplasts were resuspended in 20 ml of cold lysis buffer (50 mM KPi, pH 7.5, 200 mM Sorbitol, 1:200 dilutions of solutions P and PIC) and disrupted with 20 strokes in a pre-chilled Dounce homogenizer. Lysates were cleared by centrifuging 5 min at 500 × g. The supernatant (S_5) was subjected to a centrifugation at 13,000 × g $_{max}$ for 10 min. The resulting supernatant (S_{13}) was separated from pellet (P_{13}) and further centrifuged at 100,000 × g $_{av}$ in TLA 100.2 rotor for 1 h to generate pellet (P_{100}) and supernatant (S_{100}). The fractions were analyzed by Western blotting with IgG-HRP to detect PrA-tagged SEA complex proteins or with appropriate antibodies to visualized control proteins.

For sedimentation analysis S_{13} fractions were layered on the top of a 5–20% (w/w) sucrose gradient in 50 mM KPi pH 7.5, 1:1000 dilutions of solutions P and PIC and run at 100,000 × g $_{av}$, 7 h 40 min in SW32Ti rotor at 5 °C. 2 ml fractions were collected from the top of the gradient and the percentage of sucrose was measured in each fraction by refractometry. Fractions were precipitated by adjusting to a final concentration of 0.03% sodium deoxycholate and 7.2% trichloroacetic acid (TCA), the pellets were resuspended, loaded on SDS-PAGE and subsequently analyzed by Western blot with IgG – horseradish peroxidase (HRP) antibody. The relative band intensity in each fraction of the blot was further correlated with the percentage of sucrose and sedimentation coefficients were determined according to the equation described at (43). The empirical relationship between sedimentation coefficient and molecular mass of the proteins M = $(S/0.00242)^{1.49}$ was used to determine molecular mass at the peak fractions.

Functional Tests—For growth tests at different temperatures and pH (Table supplemental Table S6), yeast were grown to mid-log phase in YPD, 10-times serial dilutions were prepared and plated either on YPD plates placed at various temperatures, YPD plates complemented with 50 nM rapamycin or on YPD plates adjusted to different pH with 50 mM MES/MOPS and/or to 50 mM or 100 mM CaCl$_2$. Plates were incubated at 30 °C for 2 days. For hypotonic stress (supplemental Table S6), yeast were labeled with FM4 – 64 (44), resuspended in water and observed under the microscope. To test the expression of indicated vacuole and exocytic markers (supplemental Table S6), whole-cell lysates from wild type and deletion strains were prepared and tested by Western blotting with the following antibodies: anti-Vph1, anti-Vma2, anti-Cpy1, anti-Alp1, anti-Vps10, anti-Por1, anti-PGK1 (Invitrogen/Molecular Probes (Carlsbad, CA) A-6426, A-6427, A-6428, A-6458, A-21274, A-6449, A-6457). For endocytosis tests (supplemental Table S6), yeast strains were transformed with plasmids, carrying GFP versions of different endocytic markers, and observed under the microscope. In addition, whole cell extracts were prepared from transformed cells and tested by Western blotting with anti-GFP antibody. For the survival test of *sea2-sea4* double deletion strains, they were grown in nitrogen deficient media

for 7 days, aliquoted out and plated to YPD plates and surviving colonies counted after 2 days of growth at 30 °C (see Fig. 8B). To test autophagy in wild type and deletion strains of SEA complex proteins, the strains were transformed with GFP-ATG8 plasmid, grown in dropout media without uracil till mid-log phase and shifted to SD-N media. Samples for Western blotting with anti-GFP antibody were taken between 45 min and 20 h of starvation. Microscope observations were performed after 20 h of starvation.

RESULTS

Identification of a Novel Complex Associated with Seh1—Affinity isolates of tagged Seh1, a protein with a β-propeller fold and one of the members of the Nup84 subcomplex, copurified with four high-molecular-weight proteins (Yjr138p (Iml1), Yol138p, Ydr128p, and Ybl104p) that do not localize to the NPC (10). These interactions were preserved even under conditions in which only tightly associated nups, *i.e.* members of the Nup84 subcomplex, remained bound to Seh1 (Fig. 1). To reflect their association with Seh1, these proteins were given a common name, Sea (for *Seh1-a*ssociated). Accordingly, we here term Yjr138p (Iml1) as Sea1, Yol138p as Sea2, Ydr128p as Sea3, and Ybl104p as Sea4.

All four Sea proteins are nonessential and their genes are largely uncharacterized. Tagged versions of each of Sea1–Sea4 copurified with each other, with Seh1, and with another three proteins—Sec13, Npr2, and Npr3 (Fig. 1; supplemental Table S1 and supplemental Table S2). Sec13 is a bona fide nucleoporin and, together with Seh1, is a member of the Nup84 subcomplex (10, 45). In addition, Sec13 interacts with Sec31 in COPII coated vesicles (13–15). However, we did not find other nups or members of COPII vesicles associated with Seas, suggesting that this group of proteins forms a novel and distinct complex, separate from either the NPC or COPII coats.

Npr2 and Npr3 have recently been identified in a genome-wide screen as specific amino acid upstream regulators of TORC1 kinase (46). These two proteins interact with each other and form an evolutionarily conserved complex (46). Npr2 and Npr3 were also associated with Seh1 under stringent immunoprecipitation conditions (Fig. 1, supplemental Table S2). To test the specificity of Npr2 and Npr3 interactions with Seas, reciprocal immunoprecipitation experiments were performed by purifying PrA-tagged Npr2 and Npr3 from yeast lysates. We have found that Npr2 and Npr3 copurified with each other together with Seh1, Sea1, Sea3, and Sea4, though without detectable amounts of Sec13 and Sea2 (Fig. 1, supplemental Table S2). Our results are supported with the data from recent genome-wide genetic interaction surveys (47). Seh1 and Sec13 are involved in a negative synthetic genetic interaction with Sea3; in addition Seh1 interacts with Sea4 (47). The global analysis of the protein kinase and phosphatase interaction network revealed that Sea1-Sea4, Npr2, Npr3, and Seh1 are phosphorylated, and two kinases, MCK1 and KIN2, play a major role in this (48). As a consequence, these proteins form a separate and distinct cluster in the
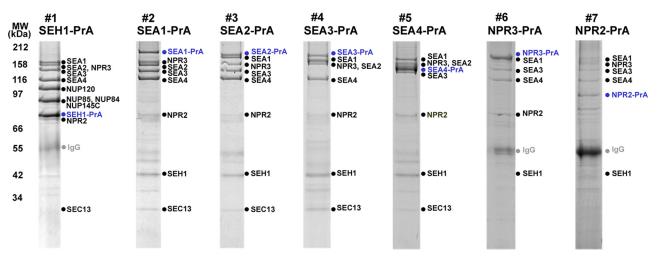
FIG. 1. **Identification of the Seh1 associated complex.** Immunoprecipitation of Protein A-tagged proteins (indicated in blue) was performed as described under "Experimental Procedures." SEA complex proteins and their partners were resolved by SDS-PAGE and visualized by Coomassie blue. Proteins identified by mass spectrometry (supplemental Table S2) are listed to the right of the gel lanes (IgG contaminant is indicated in gray). Molecular weight markers are indicated to the left of the panel. Each individual gel image was differentially scaled along its length so that its molecular mass standards aligned to a single reference set of molecular mass standards. Contrast was adjusted to improve visibility. All original gel figures are available upon request.

interaction network formed by these enzymes. Together, these data suggest that Sea1–Sea4, Seh1, Sec13, Npr2 and Npr3 are members of a novel complex which we designated as the SEA complex.

Sea Proteins Contain Structural Features Present in Intracellular Trafficking Complexes—Seh1 and Sec13 have so far been demonstrated only as part of membrane coating assemblies. In the NPC, both proteins are members of the Nup84 complex, composed of several coat proteins (3). In addition Sec13, together with Sec31, forms the structural unit of the COPII cage (13, 15). To explore whether the SEA proteins also resemble proteins found in coating complexes, we analyzed sequences and predicted fold composition for their constituent protein domains. We previously used a combined computational and biochemical approach (protease accessibility laddering, PAL) to investigate the folds for yeast and vertebrate nups, which allowed us to uncover an evolutionary link between the NPC and coated vesicles (3, 4, 23). A similar methodology was also applied here, which detected unexpected fold arrangements for *S. cerevisiae* Sea1–Sea4 and its human orthologs (Fig. 2, Fig. 3; supplemental Tables S3 and S4).

Sea1 appears to be a multidomain protein carrying an N-terminal Cdc48-like domain found in several AAA$^+$ ATPases, such as Sec18/NSF (49), immediately followed by a vWA-like domain, that is present in many membrane interacting proteins, including Sec23 of COPII vesicles (50). The central region of Sea1 (residues ~500–800) is predicted to be largely disordered and, consistent with this, is readily accessible to proteases (Fig. 2, Fig. 3*A*; supplemental Table S4). The C terminus of Sea1 contains an extended region with uncertain secondary structure predictions, followed by a DEP domain. Sea1 appears to be the first example of a protein with this

particular arrangement of putative membrane interacting domains.

Analysis of Sea2 and Sea3 revealed topologies similar to each other. These proteins contain N-terminal WD-40 repeats arranged into β-propeller structures, relatively disordered central regions and C-terminal RING motifs (Fig. 2 and supplemental Table S3). In addition Sea3 contains an RWD domain that is enriched in β-sheets and common in proteins containing RING motifs and WD-40 repeats (51). The RWD domain significantly resembles that of ubiquitin-conjugating E2 enzymes (52), however its enzymatic activity has never been demonstrated. Although analysis predicts only few structural elements in the central part of Sea2 and Sea3, PAL (23) shows that this region is not accessible to proteases and therefore is different from the disordered region of Sea1 (Fig. 3*A* and supplemental Table S4). β-sheets in the Sea2 N-terminus encompass about 500 amino acid residues; in principle, such a large number of β-sheets can be arranged into a double β-propeller structure, and several prediction servers indicated such a fold (*e.g.* 1nr0A was suggested as a template). However, we cannot reliably discriminate between the possibilities of two β-propellers and one β-propeller with additional features.

Sea4 is predicted to contain an N-terminal β-propeller fold, followed by a *s*tacked *p*airs of *a*lpha-*h*elices (SPAH)/α-solenoid region (residues ~500–850), a region of about 150 amino acid residues with unreliable secondary structure predictions and a RING motif at the C terminus (Fig. 2, Fig. 3*A*, supplemental Tables S3 and S4). The overall annotation for Sea4 is similar to that for the COPII component Sec31 (23). In fact, the Sec31 structures (PDB codes 2pm6, 2pm9) are often the best predicted templates for modeling Sea4, suggesting relatively similar structures. Sec13, which is almost exclu-
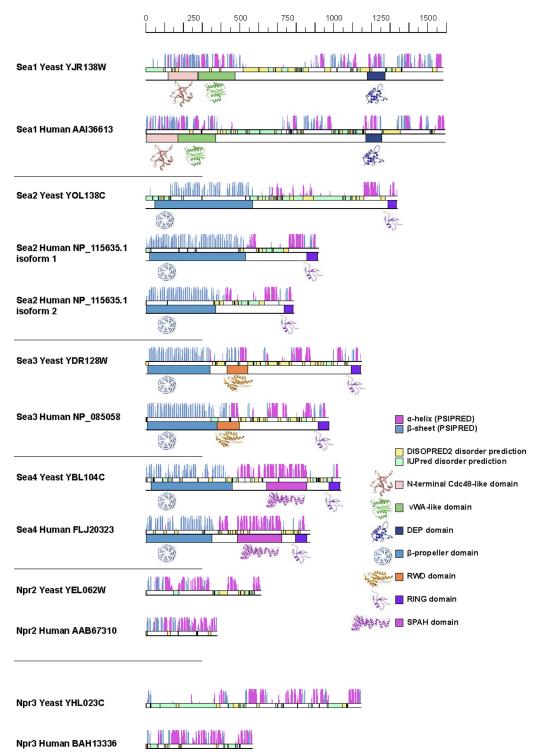
FIG. 2. **Secondary structure prediction and fold assessment of yeast *S. cerevisiae* and human SEA complex proteins.** Secondary structure predictions for each residue by PSIPRED are shown as vertical lines with α-helices colored in magenta and β-strands in cyan. The length of the column is proportional to the confidence of the secondary structure prediction (24). Disordered regions were predicted using DISOPRED2 (yellow) or IUPRED (green). Assigned folds (supplemental Table S3) are also shown, visualized with ribbon diagrams of representative atomic structures from Protein Data Bank (http://www.pdb.org).
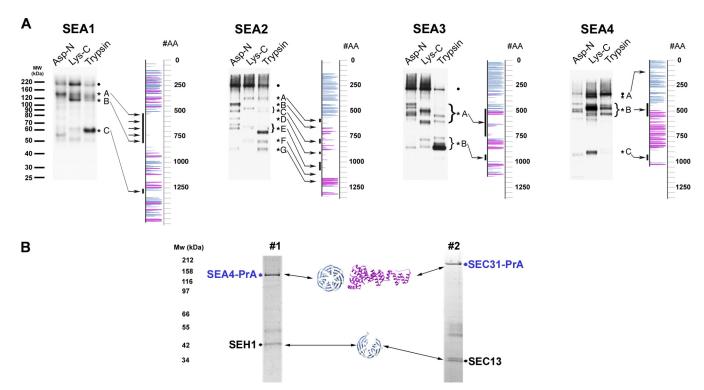
FIG. 3. **SEA complex proteins have evolutionarily conserved structural characteristics similar to membrane coats.** *A*, Protease accessibility laddering (PAL) analysis of SEA complex proteins. PAL readily detects domain boundaries and flexible loops within proteins (23). Protein A-tagged SEA proteins were purified on magnetic beads in their natively folded state. While attached to the beads, proteins were probed with proteases (Asp-D, Lys-C and Trypsin). Proteolytic fragments, containing C-terminal PrA tag were eluted and detected by immunoblotting with IgG-HRP. Shown are immunoblots of PAL digests for PrA-tagged versions of Sea1, Sea2, Sea3, and Sea4. Full-length proteins are indicated with a dot and proteolytic fragments with a star and a letter. Sites of proteolysis are marked with arrows on a secondary structure prediction map (shown to the right of each gel). Uncertainties in the precise cleavage positions are indicated by lines to the left of the map (see also supplemental Table S4). *B*, Sea4 forms a dimer with Seh1 similar to the COPII coat complex Sec31-Sec13. Note, that in this experiment Sea4-PrA was expressed in the cells deleted for Sea3 and immunoprecipitated under stringent conditions with 1 M NaCl present both in the extraction and washing buffers (see Experimental procedures). Therefore the resulting complex is different than the one shown on Fig. 1, lane #5. Sec31-PrA expressed in wild type yeast (lane #2) was immunoprecipitated as described under "Experimental Procedures." Eluted proteins were resolved on SDS-PAGE gels, stained with Coomassie blue and identified by mass spectrometry (supplemental Table S2). Arrows indicate predicted folds. Seh1 and Sec13 are indicated as 6-blade β-propeller, according to their x-ray structures (15, 76).

sively a β-propeller, forms a dimer with Sec31 (13, 15). Similarly, the Sec13 paralog Seh1 forms a dimer with Sea4 (Fig. 3B). Therefore, Sea4 and Seh1 may interact in a similar fashion to Sec31 and Sec13. Sea4 also exhibits a striking similarity to several Vps-C core complex proteins and variations, *i.e.* HOPS and CORVET (19). According to fold assignments, Vps8, Vps11, Vps18, and Vps39 of HOPS/CORVET all have an N-terminal β-propeller, followed by an α-solenoid region and a RING motif at the C terminus (19).

Our analyses were unable to assign folds for Npr2 and Npr3. However both proteins seem to contain disordered regions and uncharacterized folds, which suggests that suitable templates do not yet exist in PDB to facilitate predictions. In addition to the folds described above, all SEA complex proteins (but not Seh1 or Sec13) possess PEST motifs (supplemental Table S3) found in many rapidly degraded proteins (53).

SEA Complex Subunits are Evolutionarily Conserved—As there are several examples of opistokhont-specific (*i.e.* ani-

mals and fungi) intracellular transport proteins we asked whether the SEA complex proteins are yeast specific or more broadly conserved (54). We performed comparative genomics and phylogenetic analysis for Seas $1-4$, Npr2. and Npr3. The orthologues of these proteins in various species are mainly uncharacterized. Two evolutionary patterns emerged (Fig. 4; supplemental Fig. S1, supplemental Table S5). First, there is retention of all SEA complex members across animals and fungi, indicating that the family was fully established in the earliest members of the Opistokhonta lineage. Given representation in the Amoebozoa, (*e.g.* slime molds) this retention likely encompasses the unikonts. Importantly, representatives are found in major model organisms, including mammals, *Drosophila*, *Schizosaccharomyces pombe*, and, by definition, *S. cerevisiae*. Second, there is no evidence for any SEA complex gene in plants. Representation within the Amoebozoa, Chromalveolata, (protists and diatoms), and Excavata (other protists, including trypanosomes and Giardia) is very variable and sequence similarity weak or limited to specific segments.
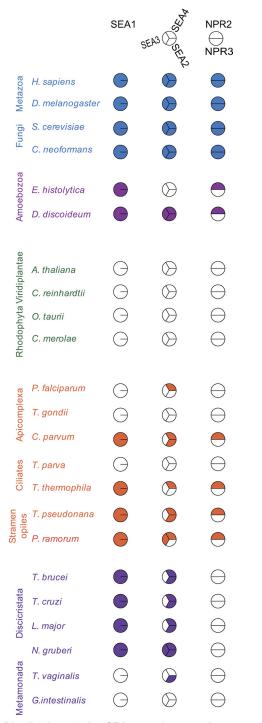
FIG. 4. **Distribution of the SEA complex proteins across the eukaryota.** Representative genomes were searched as described under "Experimental Procedures" and shown as a Coulson plot. Filled sectors represent evidence for orthologues, while open sectors indicate that no orthologue found. Individual taxa are color coded as follows: Opistokhonta, blue; Amoebozoa, light purple; Planta, green; Chromalveolata, orange; Excavata, dark purple. Lower order groupings are indicated, and a key to the factors is given at top. Factors are subdivided into three groups: Sea1, Sea2–4, Npr2, and Npr3. Accession numbers and additional data are listed in the supplemental Table S5.

Npr3 is restricted to Opistokhonta, Npr2 only additionally to amoeba and some chromalveolates, and Sea3 is restricted to Opistokhonta except for *Phytophora ramorum*, a chromalveolate, and *Naegleria gruberi*, an excavate (Fig. 4; supplemental Fig. S1, supplemental Table S5). Given evidence for at least partial representation in four eukaryotic supergroups, the most parsimonious interpretation is secondary losses, with representation in the last eukaryotic common ancestor (LCEA). However, we cannot exclude the possibility that some of these weak hits reflect recognition of polypeptides with shared secondary structures but that do not share a common ancestor. For example, it is possible that Sea3 is Opistokhonta specific. Regardless, it is clear that Seas 1−4, Npr2, and Npr3 are dispensable in many biological contexts, suggesting (i) a specialized life-style specific roles for SEA complex proteins rather than a function central to viability, and (ii) that the full complex is specific to animals and fungi.

The overall architecture of Sea proteins seems evolutionarily conserved, at least among Opistokhonts (Fig. 2). The human ortholog of Sea1, which is only 10 amino acids residues longer than its yeast counterpart, possesses a similar fold arrangement. Interestingly, human Sea2 has two isoforms, one of which is missing about 130 amino acid residues in the N-terminal part. The human orthologs of Sea2-Sea4, Npr2 and Npr3 are smaller than the yeast proteins, primarily because of deletions of the sequences, predicted to be disordered in yeast (Fig. 2).

The Proteins of the SEA Complex are Associated With the Vacuolar Membrane—A global survey of yeast GFP-tagged proteins (55) indicated that Sea1 and Sea3 were localized at the vacuolar membrane, Sea2 to the vacuole lumen, and Sea4 to the cytoplasm. These intracellular distributions are inconsistent with the proteins comprising the same complex. This discrepancy could be explained by low expression levels of the SEA complex proteins, which makes the task of their accurate localization challenging. Indeed, the relative abundance of the SEA complex components annotated in SGD is estimated to be between 200 and 600 molecules per cell.

C-terminal GFP-tagged strains were used to re-examine the localization of the SEA complex proteins. Living cells were analyzed using a confocal-spinning disk microscope and time averaged distribution of fluorescent proteins was obtained by a Sum Intensity Projection (Figs. 5*A*, 5*B*), in order to maximize the signal. All four GFP-tagged Sea proteins were detected mainly at the vacuole membrane (Fig. 5*B*). Remarkably, the GFP signal in the Seh1-GFP strain was detected not only at the nuclear envelope in agreement with Seh1's function as nucleoporin, but also around the vacuole membrane, although with a much lower intensity, consistent with Seh1 also being a SEA complex component (Figs. 5*A*, 5*B*). We were not able to detect a fluorescent signal for Npr3-GFP, most probably because the level of expression of this protein is below the detection limit. However, its
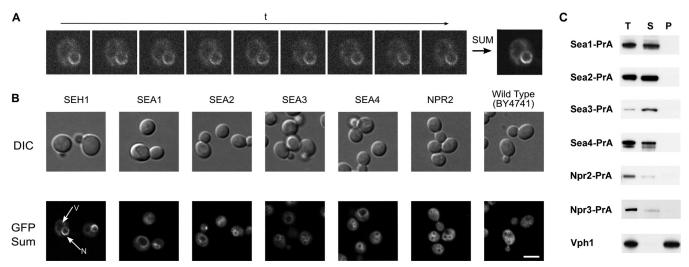
FIG. 5. **Proteins of the SEA complex are localized around vacuole membrane.** Live florescence images of the SEA complex proteins genomically expressing GFP at their C terminus. *A*, Principle of the Sum Intensity Projection (SIP) algorithm, applied for localizing Seh1-GFP. Living cells were analyzed using a confocal-spinning disk microscope with low illumination power. Intensity values on a given pixel of the image are summed over all images in the time sequence to give the final image (*right*). *B*, Yeast cells were visualized by Nomarski optics ("DIC" row). GFP signals shown in the "GFP Sum" row were obtained by SIP or Maximum Intensity Projections of image sequences (duration or number of frames) taken with high exposure times (~500 ms) to increase signal-to-noise ratio. Scale bar = 5 μm. *C*, Characterization of association of SEA complex proteins with enriched vacuole fraction. Total vacuole fractions (T) prepared from indicated PrA-tagged SEA complex proteins were treated with 0.1 M Na_2CO_3 prior to centrifugation at 100,000 $\times$ g. The resulting supernatant (S) and pellet (P) were analyzed by Western blotting with an IgG-HRP antibody. The distribution of vacuole integral membrane protein Vph1 was visualized with an anti-Vph1 antibody.

partner Npr2-GFP also exhibited vacuole membrane staining. Because Npr2 expression in the cell is low, the cytoplasmic signal observed in some cells is reasonably attributed to auto-fluorescence (cf, the wild-type cells examined under the same image acquisition setting exhibited a comparable level of cytoplasmic signal).

Sodium carbonate extraction of membranes separates integral from peripheral membrane proteins (56). We performed standard carbonate extractions of PrA-tagged SEA complex proteins from the enriched vacuole fractions, prepared from appropriate PrA-tagged strains. In contrast to the trans-membrane vacuolar protein Vph1, SEA complex proteins were found in the supernatant fraction after extraction, indicating that they are not integral to the membrane (Fig. 5*C*). Thus, all components of the SEA complex are peripherally localized at the vacuole membrane. However, because of the low level of expression of the SEA complex proteins, we cannot exclude the possibility that the SEA complex members are also present elsewhere in the cell.

SEA Complex Proteins Display Dynamic Behavior at the Vacuolar Membrane—To determine the nature of vacuole association of SEA complex proteins their localization and dynamics were observed using TIRFM with high frame rate and simultaneous dual-channel acquisition (see Experimental Procedures) (Fig. 6). This method has been used to study a number of membrane events, especially those involving the movement of vesicles and cargoes (57, 58). TIRFM was initially developed to visualize the plasma membrane-cytosol

interface because the exponentially decaying evanescent field of TIR selectively illuminates the portion of the cell within a distance of 50–100 nm from the glass coverslip. SEA complex proteins are not localized at the cellular surface and therefore the distance between their intracellular position and the coverslip (300–500 nm) is larger than in classical TIRFM setups. Nevertheless we were able to successfully apply TIRFM for analysis of Sea1-Sea4 and Seh1 dynamics in live cells, at a reasonable expense of eventual photobleaching. For image treatment we used time-lapse analysis and kymogram representation on the same data set followed by a series of adapted image processing algorithms, including mobile and background component separation (41), and patch-based nonlocal denoising (42).

Seh1-GFP, found both on the nuclear periphery and around the vacuole (see above), moves on both compartments with distinct kinetics, being more dynamic on the vacuolar membrane. To confirm that the dynamic behavior of Seh1-GFP at the vacuole membrane does not depend on the intrinsic movement of this organelle we examined the localization of the transmembrane vacuole protein Vph1. The fluorescent signal from Vph1-GFP was almost constant over the time and well restricted to the vacuole membrane, as expected for a homogeneously distributed transmembrane protein (Fig. 6). Therefore, observations on the dynamics of Seh1-GFP were specific and probably not due to motion of the vacuolar membrane itself.

Similarly to Seh1-GFP, the signal from Sea1-GFP, Sea4-GFP, or Sea4-mCherry appears as rapidly moving or blinking
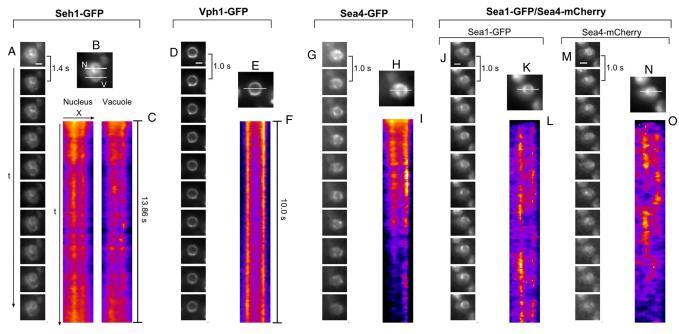
FIG. 6. **Dynamics of the SEA complex proteins.** (A, D, G, J, M): image sequence showing the dynamics of the fluorescently tagged proteins (time interval between two images is 1.4 s for Seh1 and 1.0 s for all other proteins). The dynamics of Sea1-GFP shown at (J) corresponds to the Movie S1. (B, E, H, K, N): SIP images showing the average localization of the protein with white lines indicating the regions used for generation of kymograms. Seh1-GFP localization at the nuclear envelope and at the vacuole membrane is indicated with "N" and "V", respectively. (C, F, I, L, O) Kymogram representations of the image sequences along horizontal (x) or vertical (t) lines as shown on SIP images. Intensity traces appear more blurry on the Sea4-mCherry kymogram, because of a difference in optical resolution due the red shift of the fluorescence emission spectrum of the mCherry tag compared with the GFP tag, as well as a difference in the incidence angle of the 561 nm laser used for detection of mCherry compared with the 491 nm laser (GFP detection). Scale bar = 2 μm.

punctae on the surface of the vacuole (Fig. 6, Movie S1). Sea2 and Sea3 also behave in the same manner (data not shown). Kymogram analysis confirmed that these punctae are dynamic, indicating either rotational motion or association and dissociation of proteins with the vacuolar membrane.

We next examined the behavior of two proteins of the complex, Sea1-GFP and Sea4-mCherry, expressed in the same cell. Sea1-GFP and Sea4-mCherry were partially moving together, as shown by comparisons between kymograms (Fig. 6). The overall distribution of the two proteins does not appear totally coincident and is somewhat variable between different cells, although remaining concentrated in vacuolar membrane domains (Fig. 6). The partial nature of this colocalization may reflect the fact that we are at the current limits of detection; or may be because the SEA complex is a dynamic assembly in a constant state of flux with its components; or these components may form more than one kind of SEA complex, rather like the HOPS/CORVET complexes.

Subcellular Fractionation and Biophysical Characterization of the SEA Complex Proteins—As a complement to our fluorescent localization of the SEA complex proteins, we performed subcellular fractionations of lysates prepared from strains carrying PrA-tagged versions of the SEA complex proteins (Fig. 7). Although all the SEA complex proteins are present to a minor extent in the vacuole-containing P_{13} fraction, they mainly accumulate in the small particulate P_{100}

fraction, which usually contains small membranes, (*e.g.* Golgi complex), transport vesicles, membrane associated complexes (*e.g.* coatomer-related retromer), and big complexes (*e.g.* ribosomes). Sea1, Sea3, Sea4, and Npr2 exhibit some residual presence in S_{100} (Fig. 7A). The S_{13} fractions obtained in the subcellular fractionation experiments were subjected to further fractionation over a 5–20% sucrose centrifuge gradient (Fig. 7B) and approximate S values at the peak fractions were estimated (43). Our analysis demonstrates that SEA complex proteins form two species on this gradient, corresponding to S values between 10S and 30S for the first species and at around 50S for the second species (Fig. 7C). The lower S value species might be indicative of a monomer SEA complex (~1 MDa), which is consistent with the summed molecular weights of its components, whereas the second suggests that SEA can oligomerize to form large complexes (>3 MDa). Thus, consistent with the fluorescence localization data, the SEA proteins seem to be organized into large assemblies that dynamically associate with the vacuolar surface.

Function of the SEA Complex Members in Membrane Trafficking and Autophagy—Phylogenetic analyses (see previous discussion) suggest that SEA complex proteins might be dispensable for general cell viability. Indeed, deletions of the SEA complex genes in *S. cerevisiae* did not have an effect on the ability of the mutant strains to grow at 23 °C, 30 °C, and 37 °C (supplemental Table S6). Surprisingly, even a sea2Δ, sea3Δ,
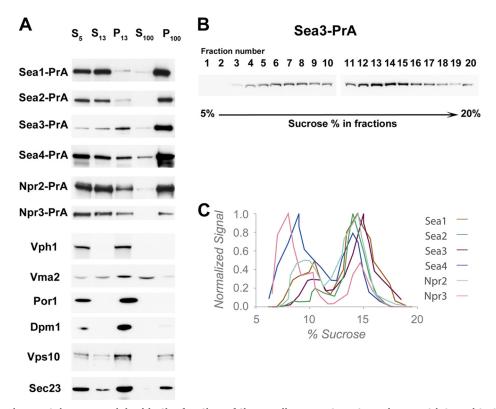
FIG. 7. **SEA complex proteins are enriched in the fraction of the small compartments and are not integral to the membrane.** *A*, Distribution of SEA complex proteins and membrane components of various organelles between different fractions generated by subcellular fractionation. The yeast cell lysates prepared from strains, containing indicated PrA-tagged SEA complex proteins were subjected to a low-force centrifugation to pellet unlysed cells and large aggregates. The cleared lysate (S_5) was further subjected to sequential centrifugation steps to generate a $13,000 \times g$ pellet (P_{13}) and supernatant (S_{13}), a $100,000 \times g$ pellet (P_{100}), and a $100,000 \times g$ supernatant (S_{100}). The P_{13} fraction contains plasma membrane and membranes of big organelles (*e.g.* nuclear, vacuolar, mitochondrial, and ER); P_{100} fraction is enriched in smaller compartments (Golgi complex, transport vesicles, and ribosomes); S_{100} fraction contains soluble cytoplasmic proteins and released peripheral membrane proteins. Samples of fractions were normalized to cell equivalents by differential loading on SDS-PAGE, which was further subjected to Western blotting and probed either with IgG-HRP to reveal PrA-tagged SEA complex proteins or with appropriate antibodies against control proteins (indicated to the *left* of the blot). Integral membrane proteins of the vacuole (Vph1), mitochondria (Por1), and ER (Dpm1) were precipitated in the P_{13} fraction. The vacuolar peripheral membrane protein Vma2 is equally distributed between P_{13} and S_{100}. Vps10, which cycles between the late-Golgi and prevacuolar endosome-like compartments, and COPII member Sec23 are found in P_{13} and P_{100}. *B*, S_{13} fractions were sedimented on a 5–20% sucrose gradient. Fractions were collected and analyzed by immunoblotting of PrA tag. Immunoblot from a typical analysis indicating a distribution between fractions of Sea3-PrA. *C*, A graph showing the sedimentation profile of six SEA complex proteins. The proteins are distributed in two sub-populations.

and sea4Δ triple deletion strain did not show growth defects at any temperature tested.

We next examined the behavior of various mutants under conditions that can affect vacuole functions (supplemental Fig. S2, supplemental Fig. S3, and supplemental Table S6). We did not detect significant defects in vacuole morphology in any deletion mutant under normal growth conditions (supplemental Table S6). Vacuole morphology and fusion upon hypotonic stress were also unaffected. In addition, the expression level of vacuole membrane proteins Vph1 and Vma2 was comparable in the wild-type and mutant strains (supplemental Fig. S2). A number of tests performed to verify vacuole pump functionality also did not reveal any significant defects (supplemental Table S6).

Given the structural connection of the SEA complex to other membrane coating assemblies or membrane tethering complexes, we tested for a possible involvement of the SEA complex in membrane trafficking, nutrition deprivation and autophagy. Endocytosis and multivesicular body sorting of selected markers were not affected in any of the depletion mutants tested (supplemental Table S6, supplemental Fig. S2, supplemental Fig. S3). This result might be explained by the fact that the SEA complex is involved in potentially redundant synthetic genetic interactions with practically the entire membrane trafficking machinery of the cell (see the following discussion). We also tested whether SEA mutants are sensitive to rapamycin treatment and nitrogen deprivation, two experimental conditions inducing the autophagic response. Growth
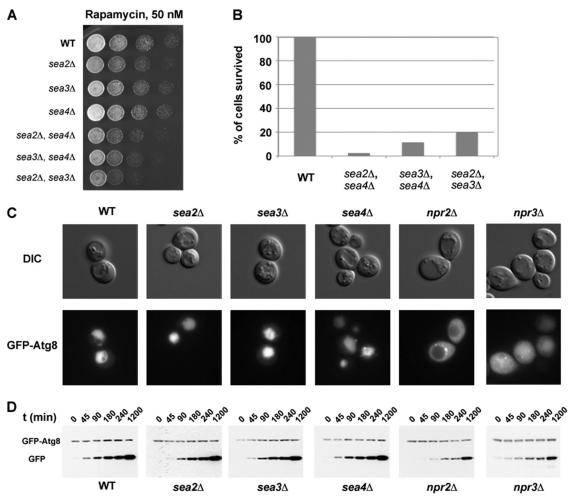
FIG. 8. **A survey of phenotypes in the SEA complex deletion strains.** *A*, Sensitivity to 50 nM rapamycin of single and double deletion strains of sea2-sea4. Indicated deletion strains were spotted in 5-fold dilution steps on YPD plates complemented with 50 nM rapamycin and grown for 4 days at 30 °C. *B*, Survival of sea2-sea4 double deletion strains after 7 days of nitrogen starvation. *C*, Wild type and indicated deletion strains transformed with a plasmid containing GFP-ATG8 were grown as described under "Experimental Procedures" and examined under a fluorescent microscope. Scale bar = 5 μm. *D*, Strains were grown as described under "Experimental Procedures". Samples were taken at indicated time points and analyzed by Western blotting with anti-GFP antibody.

of single deletion strains of SEA2–SEA4 was not affected by rapamycin treatment. However, double deletion strains exhibited significantly increased sensitivity to this reagent (Fig. 8*A*); survival of double deletion strains after 7 days of starvation was reduced in comparison with the wild type (Fig. 8*B*). We further transformed several SEA complex deletion strains with a plasmid, coding for GFP-ATG8 (59)—a classical marker for general autophagy (60). Upon lysis of autophagic bodies containing GFP-Atg8, the GFP moiety is proteolytically removed from Atg8 in the vacuole lumen. The released GFP moiety remains relatively stable from vacuolar hydrolysis, and readily detected by fluorescence microscopy. Accordingly the appearance of free GFP on Western blots represents lysis of the membrane of the autophagic body and breakdown of the cargo. Following nitrogen starvation for 20 h the GFP signal was detected in the vacuole in the wild-type cells and in the deletion mutants of SEA2, SEA3, and SEA4 (Fig. 8*C*). How-

ever, GFP-Atg8 was blocked in the cytoplasm in the npr2Δ strain and equally distributed between the vacuole and the cytoplasm in the npr3Δ strain. The analysis by Western blot of GFP-Atg8 maturation was in agreement with fluorescent observations (Fig. 8*D*). Therefore, Npr2 and Npr3 are implicated in the general autophagy pathway. This result is consistent with recent findings that both Npr2 and Npr3 are upstream regulators of the TORC1 kinase (46). Because signals indicating abundant nutritional and trophic support activate TORC1 (and deactivate autophagy), signals of starvation or other stressors inhibit TORC1 (and activate autophagy). Accordingly, in the absence of Npr2 and Npr3 TORC1 is hyperactive, and therefore autophagy is impaired (Figs. 8*C*, 8*D*). This result suggests that members of the SEA complex might be required in the autophagy pathway.

Genetic interactions provide valuable information about function of separate proteins and their complexes. In the

Gene name	Function
Amino acid biogenesis and sorting	
GDH1, GDH2; EGO complex (GTR1, MEH1, SLM4); **LST4**, LST8; RSP5, BUL2	Gap1 sorting
AAT1, ASN1, **HOM2**, HOM3, **HOM6, THR4**, SUL2, MET1, MET3, MET6, MET12, MET14, MET30, MET31	Aspartate family biosynthesis (aspartate, asparagine, theronine, methionine)
SER1, **SER2,** CIT1, ICL1, GCV1, SHM2	Serine and glycine biosynthesis
ARO1, ARO2, ARO4, ARO7, ARO80, TRP2, TRP3	Chorismate and tryptophan biosynthesis
BAT1, ILV1, ILV3, ILV6, LEU4	Leucine, isoleucine, valine biosynthesis
GDH1, GDH2, IDH1, IDH2, LST8, URE2	Glutamate and glutamine biosynthesis
Membrane trafficking and autophagy	
AVO2, BIT61, LST8, TOR1, TOR2, SLM2, TCO89	TOR1/2 complexes (response to nutrient availability and cellular stresses)
GTR1, MEH1, SLM4	EGO complex (activates TORC in amino-acid sensitive manner; Gap1 sorting)
ATG3, ATG4, ATG11, ATG12, ATG14, ATG15, ATG21, ATG22, ATG23, ATG27	Autophagy
VPS8, VPS16, VPS18, VPS33, VPS41	HOPS/CORVET (membrane trafficking, endosome and vacuole fusion)
CCZ1, MON1, VAM3, VAM6, VAM7, YPT7, YCK3; VPS9, VPS21	HOPS and autophagosome tethering, docking and fusion with the vacuole; CORVET fusion with endosomes
PEP8, VPS5, VPS17, VPS29, VPS35	Retromer complex (endosome-to-TGN cargo retrieval)
COG3, GOG5, GOG6, COG7, COG8	Conserved oligomeric Golgi complex (fusion of transport vesicles to Golgi compartments)
VPS23, VPS26, VPS37; VPS25; VPS2, VPS24	ESCRTI; ESCRTII; ESCRTIII (endosomal sorting complex)
Ubiquitination	
RAD6, UBC4, UBC6, UBC7, UBC8, UBC12, **PEX4**	Ubiquitin conjugating enzymes (E2)
ASR1, BRE1, GID2, PIB1, RAD5, RAD18, SAN1, SLX8, UBR1, **UBR2**	Single subunit ubiquitin ligases of RING family (E3)
HUL4, MMS1, RSP5, TOM1, UFD2	Single subunit non-RING ubiquitin ligases (E3)
GID1, GID2, GID4, GID5, GID8, GID9	GID complex - multisubunit E3 ligase, carbohydrate (FBP) methabolism
CDC4, DIA2, SAF1, HRT3, MDM30, MET30, YLR224W	F-box proteins of SCF ubiquitin ligase complexes
UBP1, UBP2, UBP3, UBP6, UBP7, UBP8, UBP9, UBP14, UBP16	Ubiquitin proteases
BUL2, CDC48, DMA2, ELA1, MUB1, PRE9, UBX3, UBX4, UBX5, UBX6	Factors regulating ubiquitination

recent genome-wide pairwise fitness screen covering approximately one-third of all potential genetic interactions in yeast, when a seh1 deletion strain and a sec13–1 temperature sensitive mutant were used as queries, Sea3, Sea4, and Npr3 were detected as hits (47). We extracted and analyzed information concerning the SEA complex from the genetic network created in this study (Table I), which showed that the five SEA complex members that appeared in the screen are enriched in interactions with genes involved in a number of closely related cellular processes, such as amino acid biogenesis and sorting, membrane trafficking and autophagy (Table I).

Thus, despite the dynamic association of the SEA complex proteins to the vacuole membrane their deletion has only a minor effect on the examined vacuole functions. In contrast our results are consistent with the idea that this complex is involved in cellular responses to nutritional stresses and environment-specific conditions (Table I, *Discussion*).

DISCUSSION

The SEA Complex Belongs to a Superfamily of Coating Complexes Involved in Membrane Trafficking—Here we report a novel vacuole-associated complex that both shares common subunits with the NPC and retains a protocoatomer class β-propeller/α-solenoid structure. We previously proposed the protocoatomer hypothesis, suggesting that various coated vesicles and the scaffold of the nuclear pore complexes originated from a common evolutionary ancestor (3, 4). The Sea2-Sea4 proteins are predicted to possess a β-propeller/α-solenoid architecture characteristic of proteins that form coats around membranes and participate in membrane tethering (Table II) (3–5, 11, 15, 17, 19, 61). The SEA complex contains five proteins with β-propellers, a domain common in coating assemblies (3–5, 11, 15, 17, 19, 61), where it provides a molecular scaffold for protein interactions, facilitating oligomerization. Strikingly, Sea4 contains an N-terminal β-propel-

ler, an α-solenoid and a C-terminal RING domain, an identical organization to Vps8, Vps11, Vps18, and Vps39 proteins of the HOPS and CORVET tethering complexes (Table II) (19). Moreover Vps3, Vps16, and Vps41, additional HOPS/CORVET proteins, contain only a β-propeller and an α-solenoid, a structural arrangement shared by proteins in coated vesicles and the structural core of the NPC. Sedimentation analysis indicates that the SEA complex is present as a multi-copy assembly, similar to coat complexes and in particular the COPII coat, which exists in the cytoplasm as a pre-assembled complex (5, 7, 14, 15, 61). Remarkably, Sea4 forms a heterodimer with Seh1 (Fig. 3B), potentially analogous to the Sec13/31dimer in COPII (13, 15).

Three SEA complex subunits, Sea2, Sea3 and Sea4, have a C-terminal RING domain. The high frequency of RING domains in the SEA complex suggests that the complex may act as an E3 ligase. Although E3 activity for HOPS/CORVET has not yet been demonstrated, the RING domains of Vps8 and Vps18 are required for VPS-C function (19). Interestingly, Npr2 interacts with Grr1, the F-box component of SCF^{Grr1} E3 ubiquitin ligase (62). This particular ligase often interacts with PEST motif carrying proteins in phosphorylation dependent manner. Given that yeast SEA complex proteins are phosphorylated (48), and possess both PEST motifs and RING domains (supplemental Table S3), it will be of interest to explore the role of post-translational modifications and protein turnover on SEA complex function.

Our bioinformatic analysis indicates that the SEA complex also has proteins with structural domains involved in additional aspects of membrane organization and vesicle fusion. Thus, Sea1 possesses a domain similar to the N-terminal part of yeast Sec18 and its mammalian ortholog NSF, which belongs to a family of "Cdc48 N-terminal domain-like" proteins. Although the proteins in this family are AAA$^+$ ATPases, their N-terminal domain is not required for catalytic activity, suggesting that Sea1 is unlikely to be an ATPase. The N-terminal domain is often involved in the membrane interaction, as for example, in Sec18/NSF where it is necessary for SNAREs disassembly (63). Interestingly, SEA complex members exhibit genetic interactions with several SNAREs that reside at the vacuole membrane, including Vam3, Vam6, and Vam7, and which participate in interactions with the HOPS complex (47, 63). Another fold in Sea1 is a vWA-like domain. This domain is also found in Sec23 of COPII vesicles, where it functions as an adaptor platform for cargo selection during vesicle formation (50). Finally, Sea1 also carries a DEP domain, which mediates interactions with membrane bound receptors (64).

Taken together, the SEA complex demonstrates remarkable relatedness at the structural and compositional levels to characterized vesicle coating complexes, and appears structurally most closely related to the HOPS/CORVET tethering complexes. Moreover, the predicted structures of all the SEA complex components strongly implicate this complex in membrane-associated trafficking or regulatory events.

Multiple Roles for Seh1 and Sec13—Two evolutionary conserved β-propeller proteins in the SEA complex are also known coatomer components: Sec13 in the COPII complex, and both Sec13 and Seh1 in the NPC. First, this powerfully underscores evolutionary links between the SEA complex,

TABLE II

Summary of composition and domain architecture of various coating assemblies components. β-propeller (cyan), SPAH (magenta), and RING (purple) folds are represented schematically. Sea4 model was created by combination of ModWeb models for the β-propeller and the RING domains, and I-TASSER model for the SPAH domain (see Experimental procedures)

Complex	Proteins	Structure	Reference
COPI	α-COP		(5)
	β-COP		(5)
COPII	Sec31		(13-15, 23)
	Sec13		(15)
Clathrin	Clathrin heavy chain		(61)
NPC	Nup170, Nup157, Nup133, Nup120		(3, 4, 15, 16, 76)
	Nup192, Nup188, Nup145C, Nup85, Nup84		
	Sec13, Seh1		
IFT	Ift40, Osm4, Wdr19, Wdr35, Ift172		(17)
	Che2		
	Ift188		
HOPS/ CORVET	Vps3, Vps16		(19)
	Vps8, Vps11, Vps18, Vps41		
SEA	Sea2, Sea3		(This study)
	Sec13, Seh1		(16, 76)
	Sea4		(This study)

known vesicle coating complexes, and the NPC. Second, Seh1 has at least two distinct roles whereas Sec13, remarkably, has at least three. Sec13, but not Seh1, is an essential protein, indicating that despite these two proteins being the most closely related in the yeast genome *i.e.* paralogs, they are functionally distinct and Seh1 cannot complement Sec13. Several studies are consistent with an expanded functional repertoire for these proteins. For example, *S. cerevisiae* sec13–1 mutants exhibit significant defects in the sorting of general amino acid permease Gap1 (65). *Homo sapiens* Seh1 functions in chromosome alignment and segregation (66) and Seh1 in *Aridopsis thaliana* is found in multiple locations, including the nucleus, Golgi, and prevacuolar compartments (67). Interestingly, about 20% of genes showing synthetic genetic interactions with *S. cerevisiae* seh1 and sec13–1 are completely uncharacterized (47). Both Seh1 and Sec13 are thus examples of an increasing number of proteins that violate a "one protein, one function" dogma. Instead, these proteins are repurposed to "moonlight" in several disparate roles, carrying functionalities that are adaptable at many different places in the cell (68).

Functions of the SEA Complex—Employing a broad range of analyses we screened for potential functions for the SEA complex, using strains deleted for one or several SEA members (Fig. 8; supplemental Table S6, and supplemental Figs. S2 and S3). Surprisingly SEA complex deletion strains exhibited relatively robust growth under a broad range of tests (supplemental Table S6), suggesting that the SEA complex functions alongside other related complexes and may be redundant under numerous growth conditions. However, complete redundancy is unlikely given the retention of SEA complex subunits, especially by the animals and fungi. These observations prompted us to consider SEA complex synthetic interactions (47) and chemical genetic profiles (69). These data indicate that SEA complex members are implicated in multiple genetic interactions with genes responsible for amino acid biogenesis and sorting, membrane trafficking, autophagy, and ubiquitination (Table I).

A gene cohort involved in amino acid biosynthesis and sorting exhibits a large number of strong genetic interactions with SEA complex subunits (Table I). Notably, HOPS/CORVET belongs to this same interaction cluster (47), further underscoring the similarity between these complexes and the SEA complex. One module in the cluster is responsible for sorting of a general amino acid permease Gap1. Gap1 sorting is mediated by multiple proteins, including the EGO complex, Lst proteins, and Rsp5-Bul1-Bul2-dependent ubiquitination of Gap1 itself. All of these genes display genetic interaction with SEA subunits (Table I). Moreover, Sea2, Sea4 and Sec13 show similar homozygous co-fitness with several genes involved in Gap1 sorting (69). Another cluster of genes showing strong genetic interaction both with the SEA complex and HOPS/CORVET is responsible for biosynthesis of amino acids, especially of the homoserine, aspartate, and aromatic family

(Table I) (47). Npr2 and Npr3, and genes involved in aromatic amino acid biosynthesis, all belong to a cohort of genes implicated in resistance to environmental perturbation (69).

Our experiments also show that double deletion strains of SEA2-SEA4 demonstrate increased sensitivity to growth on poor nitrogen sources (Fig. 8B). One of the consequences of nitrogen starvation is autophagy, a process when cytoplasmic components are sequestered into autophagosomes and delivered into the vacuole/lysosome for degradation (70). SEA complex components exhibit synthetic interactions with many autophagy genes and members of complexes involved in autophagy regulation, such as HOPS, EGO, and COG (Table I) (47). In addition, Npr2 and Npr3 are upstream regulators of the TORC1 kinase (46). The Npr2 ortholog in humans—Nprl2—interacts with Pdk1 kinase (71), one of the well-defined upstream regulators of TORC1 pathway in mammalian cells. These results support our demonstration that deletion of either Npr2 or Npr3 leads to impaired autophagy (Fig. 8). Collectively, these data suggest that the SEA complex plays a role in the regulation of amino acid biosynthesis and autophagy.

Evolutionary Conservation of the SEA Complex—Except for the plants, several SEA complex subunits are broadly retained across the eukaryotes, suggesting an origin for these factors before the LCEA (1). However the full complex is only retained by animals and fungi. Although the SEA complex is probably another example of the protocoatomer expansion that gave rise to CVs, NPCs and other membrane coating, tethering, and related systems, its evolutionary history is rather distinct from most of these examples, as SEA complex subunits are rather less well retained than, for example COPI or COPII. Significantly the Sea proteins are better retained than Npr2 and Npr3, the latter lacking the protocoatomer architecture. Remarkably, HOPS members are also subjected to secondary losses, similarly to the SEA complex (72). The implication that the entire SEA complex is retained in animals and fungi underlines the functional importance of this assembly to the opistokhont supergroup. Interestingly, the Sea4 ortholog in *Drosophila* (missing oocyte, mio) is preferentially accumulated in pro-oocyte nuclei and required for the maintenance of the meiotic cycle and oocyte identity (73). The Npr2 ortholog in humans (Nprl2) has been characterized as a novel tumor suppressor (74). Low expression of Nprl2 in different types of lung cancers and other tumors was correlated with resistance to cisplatin, one of the mainstays of chemotherapy for lung cancer (75). We propose that the SEA complex is a new member of the coatomer group and provides further evidence that pre-LCEA expansion of the protocoatomer family underpins much of the functional elaboration of the endomembrane system.

[S] This article contains supplemental Tables S1 to S6 and Figs. S1 to S3, and Movie S1.

[a] To whom correspondence should be addressed: Institut Gustave Roussy, CNRS UMR 8126, 114, rue Edouard Vaillant, 94805, Villejuif, France. Tel.: +33142114920; Fax: +33142115494; E-mail: svetlana.dokudovskaya@igr.fr.

‖ These authors contributed equally to this work.

REFERENCES

1. Dacks, J. B., and Field, M. C. (2007) Evolution of the eukaryotic membrane-trafficking system: origin, tempo and mode. *J. Cell Sci.* **120,** 2977–2985
2. DeGrasse, J. A., DuBois, K. N., Devos, D., Siegel, T. N., Sali, A., Field, M. C., Rout, M. P., and Chait, B. T. (2009) Evidence for a shared nuclear pore complex architecture that is conserved from the last common eukaryotic ancestor. *Mol. Cell Proteomics* **8,** 2119–2130
3. Devos, D., Dokudovskaya, S., Alber, F., Williams, R., Chait, B. T., Sali, A., and Rout, M. P. (2004) Components of coated vesicles and nuclear pore complexes share a common molecular architecture. *PLoS Biol.* **2,** e380
4. Devos, D., Dokudovskaya, S., Williams, R., Alber, F., Eswar, N., Chait, B. T., Rout, M. P., and Sali, A. (2006) Simple fold composition and modular architecture of the nuclear pore complex. *Proc. Natl. Acad. Sci. U.S.A.* **103,** 2172–2177
5. Lee, C., and Goldberg, J. (2010) Structure of Coatomer Cage Proteins and the Relationship among COPI, COPII, and Clathrin Vesicle Coats. *Cell* **142,** 123–132
6. Bonifacino, J. S., and Glick, B. S. (2004) The mechanisms of vesicle budding and fusion. *Cell* **116,** 153–166
7. Gürkan, C., Stagg, S. M., Lapointe, P., and Balch, W. E. (2006) The COPII cage: unifying principles of vesicle coat assembly. *Nat. Rev. Mol. Cell Biol.* **7,** 727–738
8. Edeling, M. A., Smith, C., and Owen, D. (2006) Life of a clathrin coat: insights from clathrin and AP structures. *Nat. Rev. Mol. Cell Biol.* **7,** 32–44
9. Field, M. C., and Dacks, J. B. (2009) First and last ancestors: reconstructing evolution of the endomembrane system with ESCRTs, vesicle coat proteins, and nuclear pore complexes. *Curr. Opin. Cell Biol.* **21,** 4–13
10. Alber, F., Dokudovskaya, S., Veenhoff, L. M., Zhang, W., Kipper, J., Devos, D., Suprapto, A., Karni-Schmidt, O., Williams, R., Chait, B. T., Rout, M. P., and Sali, A. (2007) Determining the architectures of macromolecular assemblies. *Nature* **450,** 683–694
11. Alber, F., Dokudovskaya, S., Veenhoff, L. M., Zhang, W., Kipper, J., Devos, D., Suprapto, A., Karni-Schmidt, O., Williams, R., Chait, B. T., Sali, A., and Rout, M. P. (2007) The molecular architecture of the nuclear pore complex. *Nature* **450,** 695–701
12. Santarella-Mellwig, R., Franke, J., Jaedicke, A., Gorjanacz, M., Bauer, U., Budd, A., Mattaj, I. W., and Devos, D. P. (2010) The compartmentalized bacteria of the planctomycetes-verrucomicrobia-chlamydiae superphylum have membrane coat-like proteins. *PLoS Biol.* **8,** e1000281
13. Stagg, S. M., Gürkan, C., Fowler, D. M., LaPointe, P., Foss, T. R., Potter, C. S., Carragher, B., and Balch, W. E. (2006) Structure of the Sec13/31 COPII coat cage. *Nature* **439,** 234–238
14. Stagg, S. M., LaPointe, P., Razvi, A., Gürkan, C., Potter, C. S., Carragher, B., and Balch, W. E. (2008) Structural basis for cargo regulation of COPII coat assembly. *Cell* **134,** 474–484
15. Fath, S., Mancias, J. D., Bi, X., and Goldberg, J. (2007) Structure and organization of coat proteins in the COPII cage. *Cell* **129,** 1325–1336
16. Brohawn, S. G., Partridge, J. R., Whittle, J. R., and Schwartz, T. U. (2009) The nuclear pore complex has entered the atomic age. *Structure* **17,** 1156–1168
17. Jékely, G., and Arendt, D. (2006) Evolution of intraflagellar transport from coated vesicles and autogenous origin of the eukaryotic cilium. *Bioessays* **28,** 191–198
18. Jin, H., White, S. R., Shida, T., Schulz, S., Aguiar, M., Gygi, S. P., Bazan, J. F., and Nachury, M. V. (2010) The conserved Bardet-Biedl syndrome proteins assemble a coat that traffics membrane proteins to cilia. *Cell* **141,** 1208–1219
19. Nickerson, D. P., Brett, C. L., and Merz, A. J. (2009) Vps-C complexes: gatekeepers of endolysosomal traffic. *Curr. Opin. Cell Biol.* **21,** 543–551
20. Rout, M. P., Aitchison, J. D., Suprapto, A., Hjertaas, K., Zhao, Y., and Chait, B. T. (2000) The yeast nuclear pore complex: composition, architecture, and transport mechanism. *J. Cell Biol.* **148,** 635–651
21. Cristea, I. M., Williams, R., Chait, B. T., and Rout, M. P. (2005) Fluorescent proteins as proteomic probes. *Mol. Cell Proteomics* **4,** 1933–1941
22. Luo, Y., Li, T., Yu, F., Kramer, T., and Cristea, I. M. (2010) Resolving the composition of protein complexes using a MALDI LTQ Orbitrap. *J. Am. Soc. Mass Spectrom.* **21,** 34–46
23. Dokudovskaya, S., Williams, R., Devos, D., Sali, A., Chait, B. T., and Rout, M. P. (2006) Protease accessibility laddering: a proteomic tool for probing protein structure. *Structure* **14,** 653–660
24. McGuffin, L. J., Bryson, K., and Jones, D. T. (2000) The PSIPRED protein structure prediction server. *Bioinformatics* **16,** 404–405
25. Dosztányi, Z., Csizmók, V., Tompa, P., and Simon, I. (2005) The pairwise energy content estimated from amino acid composition discriminates between folded and intrinsically unstructured proteins. *J. Mol. Biol.* **347,** 827–839
26. Ward, J. J., Sodhi, J. S., McGuffin, L. J., Buxton, B. F., and Jones, D. T. (2004) Prediction and functional analysis of native disorder in proteins from the three kingdoms of life. *J. Mol. Biol.* **337,** 635–645
27. Shi, J., Blundell, T. L., and Mizuguchi, K. (2001) FUGUE: sequence-structure homology recognition using environment-specific substitution tables and structure-dependent gap penalties. *J. Mol. Biol.* **310,** 243–257
28. Lobley, A., Sadowski, M. I., and Jones, D. T. (2009) pGenTHREADER and pDomTHREADER: new methods for improved protein fold recognition and superfamily discrimination. *Bioinformatics* **25,** 1761–1767
29. Kelley, L. A., and Sternberg, M. J. (2009) Protein structure prediction on the Web: a case study using the Phyre server. *Nat. Protoc* **4,** 363–371
30. Karplus, K. (2009) SAM-T08, HMM-based protein structure prediction. *Nucleic Acids Res.* **37,** W492–497
31. Pieper, U., Eswar, N., Webb, B. M., Eramian, D., Kelly, L., Barkan, D. T., Carter, H., Mankoo, P., Karchin, R., Marti-Renom, M. A., Davis, F. P., and Sali, A. (2009) MODBASE, a database of annotated comparative protein structure models and associated resources. *Nucleic Acids Res.* **37,** D347–354
32. Zhang, Y. (2007) Template-based modeling and free modeling by I-TASSER in CASP7. *Proteins* **69 Suppl 8,** 108–117
33. Bateman, A., Birney, E., Durbin, R., Eddy, S. R., Howe, K. L., and Sonnhammer, E. L. (2000) The Pfam protein families database. *Nucleic Acids Res.* **28,** 263–266
34. Shen, M. Y., and Sali, A. (2006) Statistical potential for assessment and prediction of protein structures. *Protein Sci* **15,** 2507–2524
35. Gabernet-Castello, C., Dacks, J. B., and Field, M. C. (2009) The single ENTH-domain protein of trypanosomes; endocytic functions and evolutionary relationship with epsin. *Traffic* **10,** 894–911
36. Smith, T. F., and Waterman, M. S. (1981) Identification of common molecular subsequences. *J. Mol. Biol.* **147,** 195–197
37. Henikoff, S., and Henikoff, J. G. (1992) Amino acid substitution matrices from protein blocks. *Proc. Natl. Acad. Sci. U.S.A.* **89,** 10915–10919

38. Huelsenbeck, J. P., and Ronquist, F. (2001) MRBAYES: Bayesian inference of phylogenetic trees. *Bioinformatics* **17,** 754–755

39. Guindon, S., and Gascuel, O. (2003) A simple, fast, and accurate algorithm to estimate large phylogenies by maximum likelihood. *Syst. Biol.* **52,** 696–704

40. Stamatakis, A., Hoover, P., and Rougemont, J. (2008) A rapid bootstrap algorithm for the RAxML Web servers. *Syst. Biol.* **57,** 758–771

41. Chessel, A., Cinquin, B., Bardin, S., Salamero, J., and Kervrann, C. (2009) Computational geometry-based scale-space and modal image decomposition application to light video-microscopy imaging. *SSVM'09 proceedings. Lecture Notes Computer Sci.* **5567,** 770–781

42. Boulanger, J., Kervrann, C., Bouthemy, P., Elbau, P., Sibarita, J. B., and Salamero, J. (2010) Patch-based nonlocal functional for denoising fluorescence microscopy image sequences. *IEEE Trans. Med. Imaging* **29,** 442–454

43. McEwen, C. R. (1967) Computation of density distributions in solutions at sedimentation equilibrium. *Anal. Biochem.* **19,** 23–39

44. Vida, T. A., and Emr, S. D. (1995) A new vital stain for visualizing vacuolar membrane dynamics and endocytosis in yeast. *J. Cell Biol.* **128,** 779–792

45. Siniossoglou, S., Lutzmann, M., Santos-Rosa, H., Leonard, K., Mueller, S., Aebi, U., and Hurt, E. (2000) Structure and assembly of the Nup84p complex. *J. Cell Biol.* **149,** 41–54

46. Neklesa, T. K., and Davis, R. W. (2009) A genome-wide screen for regulators of TORC1 in response to amino acid starvation reveals a conserved Npr2/3 complex. *PLoS Genet.* **5,** e1000515

47. Costanzo, M., Baryshnikova, A., Bellay, J., Kim, Y., Spear, E. D., Sevier, C. S., Ding, H., Koh, J. L., Toufighi, K., Mostafavi, S., Prinz, J., St Onge, R. P., VanderSluis, B., Makhnevych, T., Vizeacoumar, F. J., Alizadeh, S., Bahr, S., Brost, R. L., Chen, Y., Cokol, M., Deshpande, R., Li, Z., Lin, Z. Y., Liang, W., Marback, M., Paw, J., San Luis, B. J., Shuteriqi, E., Tong, A. H., van, Dyk, N., Wallace, I. M., Whitney, J. A., Weirauch, M. T., Zhong, G., Zhu, H., Houry, W. A., Brudno, M., Ragibizadeh, S., Papp, B., Pál, C., Roth, F.P., Giaever, G., Nislow, C., Troyanskaya, O. G., Bussey, H., Bader, G. D., Gingras, A. C., Morris, Q. D., Kim, P. M., Kaiser, C. A., Myers, C. L., Andrews, B. J., and Boone, C. (2010) The genetic landscape of a cell. *Science* **327,** 425–431

48. Breitkreutz, A., Choi, H., Sharom, J. R., Boucher, L., Neduva, V., Larsen, B., Lin, Z. Y., Breitkreutz, B. J., Stark, C., Liu, G., Ahn, J., Dewar-Darch, D., Reguly, T., Tang, X., Almeida, R., Qin, Z. S., Pawson, T., Gingras, A.C., Nesvizhskii, A.I., and Tyers, M. (2010) A global protein kinase and phosphatase interaction network in yeast. *Science* **328,** 1043–1046

49. Babor, S. M., and Fass, D. (1999) Crystal structure of the Sec18p N-terminal domain. *Proc. Natl. Acad. Sci. U.S.A.* **96,** 14759–14764

50. Bi, X., Corpina, R. A., and Goldberg, J. (2002) Structure of the Sec23/24-Sar1 pre-budding complex of the COPII vesicle coat. *Nature* **419,** 271–277

51. Doerks, T., Copley, R. R., Schultz, J., Ponting, C. P., and Bork, P. (2002) Systematic identification of novel protein domain families associated with nuclear functions. *Genome Res.* **12,** 47–56

52. Nameki, N., Yoneyama, M., Koshiba, S., Tochio, N., Inoue, M., Seki, E., Matsuda, T., Tomo, Y., Harada, T., Saito, K., Kobayashi, N., Yabuki, T., Aoki, M., Nunokawa, E., Matsuda, N., Sakagami, N., Terada, T., Shirouzu, M., Yoshida, M., Hirota, H., Osanai, T., Tanaka, A., Arakawa, T., Carninci, P., Kawai, J., Hayashizaki, Y., Kinoshita, K., Güntert, P., Kigawa, T., and Yokoyama, S. (2004) Solution structure of the RWD domain of the mouse GCN2 protein. *Protein Sci.* **13,** 2089–2100

53. Rechsteiner, M., and Rogers, S. W. (1996) PEST sequences and regulation by proteolysis. *Trends Biochem. Sci.* **21,** 267–271

54. Field, M. C., Gabernet-Castello, C., and Dacks, J. B. (2007) Reconstructing the evolution of the endocytic system: insights from genomics and molecular cell biology. *Adv. Exp. Med. Biol.* **607,** 84–96

55. Huh, W. K., Falvo, J. V., Gerke, L. C., Carroll, A. S., Howson, R. W., Weissman, J. S., and O'Shea, E. K. (2003) Global analysis of protein localization in budding yeast. *Nature* **425,** 686–691

56. Fujiki, Y., Hubbard, A. L., Fowler, S., and Lazarow, P. B. (1982) Isolation of intracellular membranes by means of sodium carbonate treatment: application to endoplasmic reticulum. *J. Cell Biol.* **93,** 97–102

57. Axelrod, D. (2008) Chapter 7: Total internal reflection fluorescence microscopy. *Methods Cell Biol.* **89,** 169–221

58. Simon, S. M. (2009) Partial internal reflections on total internal reflection fluorescent microscopy. *Trends Cell Biol.* **19,** 661–668

59. Bugnicourt, A., Mari, M., Reggiori, F., Haguenauer-Tsapis, R., and Galan, J. M. (2008) Irs4p and Tax4p: two redundant EH domain proteins involved in autophagy. *Traffic* **9,** 755–769

60. Klionsky, D. J., Cuervo, A. M., and Seglen, P. O. (2007) Methods for monitoring autophagy from yeast to human. *Autophagy* **3,** 181–206

61. Fotin, A., Cheng, Y., Sliz, P., Grigorieff, N., Harrison, S. C., Kirchhausen, T., and Walz, T. (2004) Molecular model for a complete clathrin lattice from electron cryomicroscopy. *Nature* **432,** 573–579

62. Spielewoy, N., Guaderrama, M., Wohlschlegel, J. A., Ashe, M., Yates, J.R., 3rd, and Wittenberg, C. (2010) Npr2, yeast homolog of the human tumor suppressor NPRL2, is a target of Grr1 required for adaptation to growth on diverse nitrogen sources. *Eukaryot Cell* **9,** 592–601

63. Hong, W. (2005) SNAREs and traffic. *Biochim. Biophys. Acta* **1744,** 120–144

64. Ballon, D. R., Flanary, P. L., Gladue, D. P., Konopka, J. B., Dohlman, H. G., and Thorner, J. (2006) DEP-domain-mediated regulation of GPCR signaling responses. *Cell* **126,** 1079–1093

65. Roberg, K. J., Bickel, S., Rowley, N., and Kaiser, C. A. (1997) Control of amino acid permease sorting in the late secretory pathway of Saccharomyces cerevisiae by SEC13, LST4, LST7 and LST8. *Genetics* **147,** 1569–1584

66. Platani, M., Santarella-Mellwig, R., Posch, M., Walczak, R., Swedlow, J. R., and Mattaj, I. W. (2009) The Nup107–160 nucleoporin complex promotes mitotic events via control of the localization state of the chromosome passenger complex. *Mol. Biol. Cell* **20,** 5260–5275

67. Lee, M. H., Lee, S. H., Kim, H., Jin, J. B., Kim, D. H., and Hwang, I. (2006) A WD40 repeat protein, Arabidopsis Sec13 homolog 1, may play a role in vacuolar trafficking by controlling the membrane association of AtDRP2A. *Mol. Cells* **22,** 210–219

68. Jeffery, C. J. (2003) Moonlighting proteins: old proteins learning new tricks. *Trends Genet.* **19,** 415–417

69. Hillenmeyer, M. E., Fung, E., Wildenhain, J., Pierce, S. E., Hoon, S., Lee, W., Proctor, M., St Onge, R. P., Tyers, M., Koller, D., Altman, R. B., Davis, R. W., Nislow, C., and Giaever, G. (2008) The chemical genomic portrait of yeast: uncovering a phenotype for all genes. *Science* **320,** 362–365

70. Yang, Z., and Klionsky, D. J. (2009) An overview of the molecular mechanism of autophagy. *Curr. Top. Microbiol. Immunol.* **335,** 1–32

71. Kurata, A., Katayama, R., Watanabe, T., Tsuruo, T., and Fujita, N. (2008) TUSC4/NPRL2, a novel PDK1-interacting protein, inhibits PDK1 tyrosine phosphorylation and its downstream signaling. *Cancer Sci.* **99,** 1827–1834

72. Koumandou, V. L., Dacks, J. B., Coulson, R. M., and Field, M. C. (2007) Control systems for membrane fusion in the ancestral eukaryote; evolution of tethering complexes and SM proteins. *BMC Evol. Biol.* **7,** 29

73. Iida, T., and Lilly, M. A. (2004) missing oocyte encodes a highly conserved nuclear protein required for the maintenance of the meiotic cycle and oocyte identity in Drosophila. *Development* **131,** 1029–1039

74. Lerman, M. I., and Minna, J. D. (2000) The 630-kb lung cancer homozygous deletion region on human chromosome 3p21.3: identification and evaluation of the resident candidate tumor suppressor genes. The International Lung Cancer Chromosome 3p21.3 Tumor Suppressor Gene Consortium. *Cancer Res.* **60,** 6116–6133

75. Ueda, K., Kawashima, H., Ohtani, S., Deng, W. G., Ravoori, M., Bankson, J., Gao, B., Girard, L., Minna, J. D., Roth, J. A., Kundra, V., and Ji, L. (2006) The 3p21.3 tumor suppressor NPRL2 plays an important role in cisplatin-induced resistance in human non-small-cell lung cancer cells. *Cancer Res.* **66,** 9682–9690

76. Brohawn, S. G., Leksa, N. C., Spear, E. D., Rajashankar, K. R., and Schwartz, T. U. (2008) Structural evidence for common ancestry of the nuclear pore complex and vesicle coats. *Science* **322,** 1369–1373